MULTIFRAME BLIND DECONVOLUTION OF PASSIVE MILLIMETER WAVE IMAGES USING VARIATIONAL DIRICHLET BLUR KERNEL ESTIMATION

Javier Mateos[a], Antonio López[b], Miguel Vega[b], Rafael Molina[a], and Aggelos K. Katsaggelos[c]

a) Dpt. de Ciencias de la Computación e I. A., Univ. de Granada.
b) Dpt. de Lenguajes y Sistemas Informáticos, Univ. de Granada.
c) Dpt. of Electrical Engineering and Computer Science, Northwestern University.

ABSTRACT

Passive Millimeter Wave Images currently used to detect hidden threats suffer from low resolution, blur, and a very low signal-to-noise-ratio. These shortcomings render threat detection, both visual and automatic, very challenging. Furthermore, due to the presence of very severe noise, most of the blind image restoration methods fail to recover the system blurring kernel from a single image. In this paper we propose a robust Bayesian multiframe blind image deconvolution method that approximates the posterior distribution of the blur by a Dirichlet distribution. We show that this approach naturally incorporates the non-negativity and normalization constraints for the blur and cope well with the image noise. The performance of the proposed method is tested on both synthetic and real images.

Index Terms— passive millimeter wave imaging, blind image deconvolution, variational Dirichlet

1. INTRODUCTION

Every object with a non-zero absolute temperature emits millimeter waves, that is, waves in the range of the electromagnetic spectrum from 30 to 300 GHz which corresponds to wavelengths between 10 and 1 mm. A Passive Millimeter Wave (PMMW) image is formed by detecting the millimeter waves emitted from the objects in a scene. Clothing is transparent to millimeter-waves while many other objects block millimeter waves. Therefore, PMMW images (PMMWI) are widely used to detect objects concealed under clothing.

PMMWI are faced with a number of problems: low spatial resolution: (i) each image is around 200×60 pixels with the pixel size measured in centimeters due to the working wavelength; (ii) an extremely low signal-to-noise ratio (SNR); (iii) a low contrast due to the passive radiometry, (iv) and the presence of blur. It is not possible to precisely calibrate the system to avoid blur due to the previously mentioned problems. Due to the low quality of the images, automatic threat detection systems perform poorly and concealed objects must be detected by a human operator [1].

Denoising techniques have been applied to PMMWI using adaptive sparse representations [2], non-local mean [3], BM3D transform domain collaborative filtering [4] and adaptive manifolds [5]; to the best of our knowledge, however, there are no published results on PMMWI deconvolution. *Blind Image Deconvolution* (BID), image deconvolution in the present of an unknown blur, although it has been extensively studied (see [6–18]) it is still an open problem [19]. BID on PMMWIs usually fails to recover the blurring kernel from a single image due to the severe noise. We postulate that multiframe blind image deconvolution methods (see [20–22] and references therein) can be used to estimate the system blur, that can be used to restore the observed images, obtaining sharper images which can then be used to improve the performance of threat detection systems. Note that most multiframe methods assume multiple observations of the same scene with different blurs. However, our PMMW system captures different images that undergo the same blur degradation.

In this paper we extend the BID method in [18] to propose a robust Bayesian multiframe blind image deconvolution method that approximates the posterior distribution of the blur by a Dirichlet distribution. We show that this approach naturally incorporates the non-negativity and normalization constrains for the blur and cope well with the image noise.

The paper is organized as follows. In section 2 we model the acquisition system and introduce the utilized framework. In section 3 we adapt the variational Dirichlet formulation to blur estimation in [18] to our multiframe problem. Once the blur is estimated, it can be used in a non-blind deconvolution algorithm to estimate the restored images. In section 4, the proposed methodology is tested both on synthetic and real images. Finally, section 6 concludes the paper.

2. PROBLEM FORMULATION

Let us assume that we have access to N images captured by a single PWMMI system. Each one of the observed (degraded)

This work was sponsored in part by the Ministerio de Ciencia e Innovación under Contract TIN2013-43880-R, the European Regional Development Fund (FEDER) and a McCormick Research Catalyst Award, Northwestern University.

images $\mathbf{y}_l$ can be modeled as

$$\mathbf{y}_l = \mathbf{H}\mathbf{x}_l + \mathbf{n}_l, \quad l = 1, 2, \ldots, N, \tag{1}$$

where $\mathbf{x}_l$ is the original (unknown) image, $\mathbf{H}$ the convolution matrix obtained from the system blur kernel $\mathbf{h}$, and $\mathbf{n}_l$ the assumed zero-mean Gaussian white noise with variance σ_n^2. Note that since all images are captured by the same system, we can assume that all observations share the same blur and noise variance.

Our objective is to estimate the blur kernel $\mathbf{h}$ that characterizes the system as well as the images $\mathbf{x}_l$ to better identify any hidden object. Since there is an infinite number of pairs of kernels and images that match the model in Eq. (1), constraints (prior knowledge) on $\mathbf{x}_l$ and $\mathbf{h}$ must be added. A common way to solve the estimation problem (see [6–9,11,12]) is to alternatively solve the optimization on the image and blur. Recent published papers ([14–16, 18] for instance), however, have shown that using gradient images leads to better kernel estimation. Hence, in this work we formulate the blur estimation process in the filter space and the estimation of the N images in the image space leading to

$$\mathbf{x}_l^{k+1} = \arg\min_{\mathbf{x}_l} \frac{1}{2}\|\mathbf{H}^k\mathbf{x}_l - \mathbf{y}_l\|_2^2 + \lambda_{\mathbf{x}} R_{\mathbf{x}}(\mathbf{x}_l), \tag{2}$$
$$l = 1, 2, \ldots, N,$$

$$\mathbf{h}^{k+1} = \arg\min_{\mathbf{h}} \sum_{l=1}^{N}\sum_{i=1}^{2} \frac{1}{2}\|\nabla_i \mathbf{X}_l^{k+1}\mathbf{h} - \nabla_i \mathbf{y}_l\|_2^2 + \frac{\lambda_{\mathbf{h}}}{2} R_{\mathbf{h}}(\mathbf{h}), \tag{3}$$

$$\text{subject to} \quad \mathbf{h} \geq 0 \quad \text{and} \quad \sum_j h(j) = 1, \tag{4}$$

where k denotes iteration index, $\mathbf{H}^k$ and $\mathbf{X}_l^{k+1}$ are the convolution matrices formed by $\mathbf{h}^k$ and $\mathbf{x}_l^{k+1}$, respectively, $\nabla_i \mathbf{X}_l^{k+1}$, for $i = 1, 2$, are the matrices obtained from the horizontal ($i = 1$) and vertical ($i = 2$) gradient of the image $\mathbf{x}_l^{k+1}$, $R_{\mathbf{x}_l}$ and $R_{\mathbf{h}}$ are regularization functions, and $\lambda_{\mathbf{x}} > 0$ and $\lambda_h \geq 0$ are the regularization parameters controlling the trade-off between the data fidelity and regularization terms.

For the estimation of each one of the restored images from Eq. (2) we use the Fast Nondimensional Gaussianity Measure method proposed in [18], that combines fast convergence and good restoration results.

3. VARIATIONAL DIRICHLET

In this section we aim at obtaining the estimation of the blur in Eq. (3) with constraints in Eq. (4) assuming that $R_{\mathbf{h}}(\mathbf{h}) = \|\mathbf{h}\|_2^2$. From a Bayesian point of view, Eq. (3) can be viewed as the Maximum *a posteriori* (MAP) solution for the Gaussian conditional probability $p(\mathbf{y}|\mathbf{h}) \propto \exp(-\sum_l \sum_i \frac{1}{2\sigma_n^2}\|\nabla_i \mathbf{X}_l\mathbf{h} - \nabla_i \mathbf{y}_l\|_2^2)$ and the blur prior $p(\mathbf{h}) \propto \exp(-\frac{1}{2\sigma_h^2}\|\mathbf{h}\|_2^2)$, with $\lambda_{\mathbf{h}} = \sigma_n^2/\sigma_h^2$. A shortcoming of this approach is that the constraints in Eq. (4) cannot be integrated into the MAP formulation.

In this paper we apply the variational approach to approximate the solution in Eq. (3) by a Dirichlet distribution that is the closest one, in the Kullback-Leibler (KL) divergence sense, to the posterior distribution of the blur given the observation $p(\mathbf{h}|\mathbf{y})$. The Dirichlet probability density function is defined as (see p. 261 in [23]),

$$q_{\boldsymbol{\alpha}}(\mathbf{h}) = \frac{1}{B(\boldsymbol{\alpha})}\prod_{j=1}^{K} h(j)^{\alpha(j)-1},$$

where $\boldsymbol{\alpha} = \{\alpha(1), \alpha(1), \ldots, \alpha(K)\}$, with K the number of elements of the kernel, and $B(\boldsymbol{\alpha})$, the so called *multinomial Beta function*, with form

$$B(\alpha) = \frac{\prod_{i=j}^{K}\Gamma(\alpha(j))}{\Gamma(S_{\boldsymbol{\alpha}})},$$

with Γ denoting the *gamma* function and $S_{\boldsymbol{\alpha}} = \sum_{j=1}^{K}\alpha(j)$. Note that the support of the Dirichlet distribution is $\mathbf{h}$, $h(j) \in (0, 1)$ and $\sum_{j=1}^{K} h(j) = 1$, and the expected value for the kernel is $E[\mathbf{h}] = \boldsymbol{\alpha}/S_{\boldsymbol{\alpha}}$. Hence, the use of the Dirichlet distribution allows us to approximate $p(\mathbf{h}|\mathbf{y})$ by a distribution that incorporates the constraints in Eq. (4) without explicitly including them into the problem formulation.

Then, we aim at finding the Dirichlet distribution

$$q_{\hat{\boldsymbol{\alpha}}}(\mathbf{h}) = \arg\min_{q_{\boldsymbol{\alpha}}} KL(q_{\boldsymbol{\alpha}}(\mathbf{h}), p(\mathbf{h}|\mathbf{y})),$$

or, equivalently, finding $\hat{\boldsymbol{\alpha}}$ satisfying

$$\begin{aligned}
\hat{\boldsymbol{\alpha}} &= \arg\min_{\boldsymbol{\alpha}\geq lb} KL(q_{\boldsymbol{\alpha}}(\mathbf{h}), p(\mathbf{h}|\mathbf{y})) \\
&= \arg\min_{\boldsymbol{\alpha}\geq lb} \int q_{\boldsymbol{\alpha}}(\mathbf{h}) \log \frac{q_{\boldsymbol{\alpha}}(\mathbf{h})}{p(\mathbf{h}|\mathbf{y})} d\mathbf{h} \\
&= \arg\min_{\boldsymbol{\alpha}\geq lb} \int q_{\boldsymbol{\alpha}}(\mathbf{h}) \log \frac{q_{\boldsymbol{\alpha}}(\mathbf{h})}{p(\mathbf{y}|\mathbf{h})p(\mathbf{h})} d\mathbf{h} \\
&= \arg\min_{\boldsymbol{\alpha}\geq lb} \{E_{q_{\boldsymbol{\alpha}}}[\log q_{\boldsymbol{\alpha}}(\mathbf{h})] + \frac{1}{2}E_{q_{\boldsymbol{\alpha}}}[\mathbf{h}^T\mathbf{A}\mathbf{h}] + E_{q_{\boldsymbol{\alpha}}}[\mathbf{b}^T\mathbf{h}]\}
\end{aligned} \tag{5}$$

where

$$\mathbf{A} = \sum_{l=1}^{N}\sum_{i=1}^{2} \nabla_i \mathbf{X}_l^T \nabla_i \mathbf{X}_l + \lambda_{\mathbf{h}}\mathbf{I}$$

$$\mathbf{b} = -\sum_{l=1}^{N}\sum_{i=1}^{2} \nabla_i \mathbf{X}_l^T \nabla_i \mathbf{y}_l,$$

and $\boldsymbol{\alpha} \geq lb$ should be understood as $\boldsymbol{\alpha}$ having all its components greater or equal to lb. Although, theoretically, $\boldsymbol{\alpha} > 0$ is adequate, in practice, we need a small lower bound lb for $\boldsymbol{\alpha}$ to avoid numerical instability.

Let us now show the form of each term in Eq. (5). As shown in [23], the negentropy term has the form

$$E_{q_{\boldsymbol{\alpha}}}[\log q_{\boldsymbol{\alpha}}(\mathbf{h})] = (\boldsymbol{\alpha}-\mathbf{1})^T(\psi(\boldsymbol{\alpha})-\psi(S_{\boldsymbol{\alpha}})\mathbf{1})-\log(B(\boldsymbol{\alpha})),$$

where $\psi = \Gamma'/\Gamma$ is the *digamma* function. Making use of the expectation $E_{q_{\boldsymbol{\alpha}}(\mathbf{h})}[\mathbf{h}] = \boldsymbol{\alpha}/S_{\boldsymbol{\alpha}}$ and covariance matrix $\Sigma_{\boldsymbol{\alpha}}$ for Dirichlet distributions, see [23], we can easily obtain

$$\begin{aligned} E_{q_{\boldsymbol{\alpha}}}[\mathbf{h}^T\mathbf{A}\mathbf{h}] &= Tr(\mathbf{A}\Sigma_{\boldsymbol{\alpha}}) + E_{q_{\boldsymbol{\alpha}}(\mathbf{h})}[\mathbf{h}]^T\mathbf{A}E_{q_{\boldsymbol{\alpha}}(\mathbf{h})}[\mathbf{h}] \\ &= \frac{S_{\boldsymbol{\alpha}}\mathbf{A}_d^T\boldsymbol{\alpha} - \boldsymbol{\alpha}^T\mathbf{A}\boldsymbol{\alpha}}{S_{\boldsymbol{\alpha}}^2(S_{\boldsymbol{\alpha}}+1)} + \frac{\boldsymbol{\alpha}^T\mathbf{A}\boldsymbol{\alpha}}{S_{\boldsymbol{\alpha}}^2} \\ &= \frac{\boldsymbol{\alpha}^T\mathbf{A}\boldsymbol{\alpha} + \mathbf{A}_d^T\boldsymbol{\alpha}}{(S_{\boldsymbol{\alpha}}+1)S_{\boldsymbol{\alpha}}}, \\ E_{q_{\boldsymbol{\alpha}}}[\mathbf{b}^T\mathbf{h}] &= \frac{\boldsymbol{\alpha}^T\mathbf{b}}{S_{\boldsymbol{\alpha}}}, \end{aligned}$$

where $\mathbf{A}_d$ is the vector formed with the diagonal elements of $\mathbf{A}$, *i. e.*, $A_d(i) = A(i,i), i = 1, 2, \ldots, K$.

We note that, since the equality constraint in Eq. (4) is enforced by the used approximation, the problem in Eq. (5) can be efficiently solved by the gradient projection method [24], with the optimizations performed in [18] for a faster convergence.

Unfortunately, since the signal-to-noise ratio is extremely low for the PMMWI, the direct kernel estimation does not usually provide useful kernels even in this multiframe framework, especially when the blur has a large support. To alleviate this problem, a multiscale scheme [10] is applied in the kernel estimation step. First, the observed images are downsampled and a kernel is estimated from them at the coarsest level. Since the noise is reduced by the downsampling process and the blur size is much smaller, the kernel is better estimated. Then, for the next scale, we use an upsampled version of the kernel as a good initial point for the BID estimation and repeat the process up to the finest level. At this level, the image has full resolution and the kernel is better estimated since the initial guess is closer to the real blur.

Once the blur has been correctly estimated we can use a non-blind image deconvolution method to reconstruct each one of the images taken by the system. In this work we use the Fast Nondimensional Gaussianity Measure restoration method proposed in [18], the same method used for kernel estimation.

4. EXPERIMENTAL RESULTS

The proposed multiframe image deconvolution method has been tested on both synthetic and real images. To generate a set of synthetic PMMWIs, we used anthropomorphic silhouettes as 2D models. The size of each image is 60×120 pixels with a spatial resolution of 2 cm/pixel. Each pixel gray level in the model corresponds to its absolute temperature. Then, a PMMWI is obtained using Planck's law. Figure 1 shows examples of generated images, simulating a person with concealed objects. Each image is convolved with an Airy point spread function [25] to take into account the diffraction of the PMMW imaging system. Its parameters were set to 60cm aperture diameter of the lens and 5m for the distance to the object (silhouette).

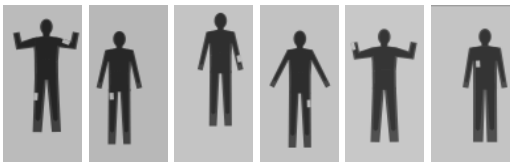

Fig. 1. Original images from the synthetic image database.

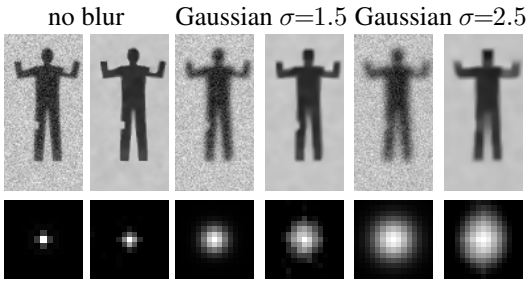

Fig. 2. (a), (c) and (d) synthetic degraded images and real blur kernel. (b), (d) and (f) their corresponding restored images and kernels using the whole set of images.

We simulated three different blur scenarios. The first one considers that the image is in focus, that is, no blur other than the diffraction effect is considered; the other two scenarios also add Gaussian blur with standard deviation 1.5 and 2.5, respectively. For each scenario, we simulated a set of 36 blurred images with Gaussian noise of SNR 10dB to simulate the internal noise of a PMMW Camera. This noise is similar to the one found in real images [26].

Starting from a 3×3 Gaussian kernel with variance 0.25 at the coarsest scale and an upsampling factor of $\sqrt{2}$, the multiscale kernel estimation method was run until the relative variation of the cost function was less than 10^{-5} or a maximum of 20 iterations was reached. The blur regularization parameter $\lambda_{\mathbf{h}}$, that controls kernel smoothness and greatly depends on the noise and the size of the image, was set to 100 for the finest level and updated accordingly for other image sizes on the multi-scale scheme. The image regularization parameter, $\lambda_{\mathbf{x}}$, controls the noise in the restoration. The larger $\lambda_{\mathbf{x}}$ is, the smoother the restoration will be and smaller the edge information for the blur estimation process we have. We noted that, for the kernel estimation process, it is better to have a smooth image than a noisy one so the high value $\lambda_{\mathbf{x}} = 0.01$ is selected.

Figure 2 shows an example of degraded and restored images, as well as the three real and estimated blurs. From the

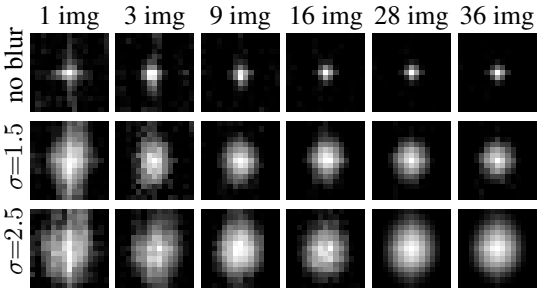

Fig. 3. Estimated kernels using different numbers of images.

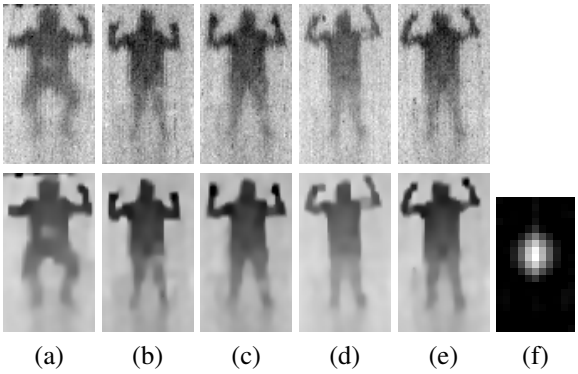

Fig. 4. Example of real images in the database. Upper row: observed images. Lower row: restored images. With a concealed object (a) on the chest, (b) on the tight, (c) on the shin, (d) on the forearm, (e) no concealed object. (f) estimated blur kernel using the 32 images in the database.

images it is clear that the method is able to successfully recover the blur and provide useful restorations to help detect concealed objects.

We also show the estimated kernels as a function of the number of images. We run the method on subsets of 1, 3, 9, 16, 28, and 36 randomly chosen images from the full set of 36 images. Figure 3 shows the estimated kernels for the different blur scenarios considered. Numerical results are shown in Table 1. From this table it is clear that the larger the number of images, the higher the mean ISNR is, meaning that a better blur estimate is obtained. However, using more than 28 images there is a only marginal increase in mean ISNR.

We also tested our method on a set of 32 real PMMWI captured with the same camera. The dataset contains images of different subjects with concealed objects on different body parts (chest, arms and legs) and also contains images of subjects without any hidden object. A noise variance value of 150 was estimated from background images. These images were captured during the same session when the blurred images were taken. The upper row of figure 4 shows an example of the images in the database. The lower row of figure 4 shows the corresponding restored images using the whole database to estimate the blur kernel, shown in Fig. 4f. We note that

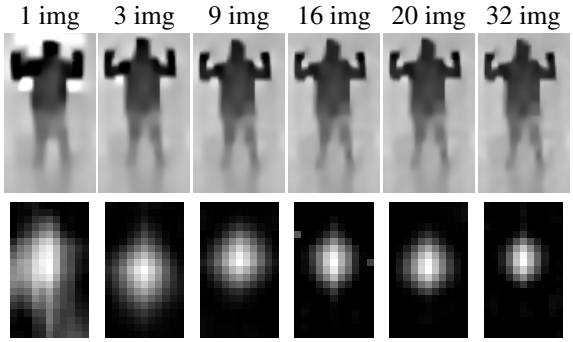

Fig. 5. Restored images (upper row) and estimated blur (lower row) when different image numbers are used for blur estimation.

Table 1. Mean ISNR for the whole image database when different number of images is used for the blur kernel estimation.

	Number of images					
blur	1	3	9	16	28	36
no blur	-0.92	0.73	4.33	6.89	7.46	7.72
$\sigma^2 = 1.5$	2.69	3.63	4.46	4.12	4.50	4.56
$\sigma^2 = 2.5$	2.90	2.76	3.13	3.18	3.27	3.27

the method successfully removed the noise from the images which are now crisp. The concealed objects are now much more clearly visible. The obtained blur resembles the blur obtained from the synthetic images which validates the proposed approach. We run the method on different subsets of randomly chosen images. Looking at the obtained blur kernels (see Fig. 5) we can see that not much improvement is obtained when more than 20 images are used.

5. ACKNOWLEDGEMENTS

We would like to acknowledge the use of the real PMMWIs provided by Wavecamm company (http://wavecamm.com/).

6. CONCLUSIONS

We have presented a multiframe blind image deconvolution method able to estimate the blur kernel in PMMWI. The proposed variational Dirichlet methodology approximates the posterior distribution of the blur by a Dirichlet distribution. The non-negativity and normalization blur constraints are inherent properties of the Dirichlet distribution and, hence, they are naturally imposed to the blur. Experiments show that the proposed method estimates the blur precisely even when the noise is very severe. Using the proposed restoration method in combination with classification techniques will improve the performance of PMMWI detection systems.

7. REFERENCES

[1] I. Gómez Maqueda, N. Pérez de la Blanca, R. Molina, and A. K. Katsaggelos, "Fast millimetre wave threat detection algorithm," in *EUSIPCO*, 2015, pp. 599–603.

[2] Q. Zhang, Y. Fu, L. Li, and J. Yang, "A millimeter-wave image denoising method based on adaptive sparse representation," in *ICCP*, Oct. 2011, pp. 652 –655.

[3] Y. Li and Y. Li, "Passive millimeter-wave image denoising based on improved algorithm of non-local mean," *Int. J. of Adv. in Computing Tech.*, vol. 4, no. 10, 2012.

[4] Y. Li, Y. Li, H. Su, Z. Li, F. Qinghui, Z. Li, and Z. Shujin, "Passive millimeter wave image denoising based on improved version of BM3D," *Advances in Information Sciences & Service Sciences*, vol. 4, no. 22, 2012.

[5] S. Zhu, Y. Li, J. Chen, and Y. Li, "Passive millimeter wave image denoising based on adaptive manifolds," *Progress In Electromagnetics Research B*, vol. 57, pp. 63–73, 2014.

[6] R. Molina, A. K. Katsaggelos, J. Abad, and J. Mateos, "A Bayesian approach to blind deconvolution based on Dirichlet distributions," in *ICASSP*, 1997.

[7] J. H. Money and S. H. Kang, "Total variation minimizing blind deconvolution with shock filter reference," *Image and Vision Comp.*, vol. 26, pp. 302–314, 2008.

[8] C. L. Likas and N. P. Galatsanos, "A variational approach for Bayesian blind image deconvolution," *IEEE Trans. Signal Process.*, vol. 52, no. 8, pp. 2222–2233, 2004.

[9] R. Molina, J. Mateos, and A. K. Katsaggelos, "Blind deconvolution using a variational approach to parameter, image, and blur estimation," *IEEE Trans. Image Process.*, vol. 15, no. 12, pp. 3715–3727, 2006.

[10] R. Fergus, B. Singh, A. Hertzmann, S. T. Roweis, and W. T. Freeman, "Removing camera shake from a single photograph," *ACM Trans. Graph*, vol. 25, no. 3, 2006.

[11] J. Cai, H. Ji, C. Liu, and Z. Shen, "Blind motion deblurring from a single image using sparse approximation," in *CVPR*, 2009.

[12] M. S. C. Almeida and M. A. T. Figueiredo, "Blind image deblurring with unknown boundaries using the alternating direction method of multipliers," in *ICIP*, 2013.

[13] S. Cho and S. Lee, "Fast motion deblurring," *ACM Trans. Graph*, vol. 28, no. 5, 2009.

[14] A. Levin, Y. Weiss, F. Durand, and W. T. Freeman, "Efficient marginal likelihood optimization in blind deconvolution," in *CVPR*, 2011, pp. 2657 –2664.

[15] S. Babacan, R. Molina, M. Do, and A. Katsaggelos, "Bayesian blind deconvolution with general sparse image priors," in *ECCV*, 2012.

[16] L. Xu, S. C. Zheng, and J. Y. Jia, "Unnatural l0 sparse representation for natural image deblurring," in *CVPR*, 2013.

[17] T. Yue, S. Cho, J. Wang, and Q. Dai, "Hybrid image deblurring by fusing edge and power spectrum information," in *ECCV*, 2014, pp. 79–93.

[18] X. Zhou, J. Mateos, F. Zhou, R. Molina, and A. K. Katsaggelos, "Variational Dirichlet blur kernel estimation," *IEEE Trans. Image Process.*, vol. 24, pp. 5127–5139, 2015.

[19] P. Ruiz, X. Zhou, J. Mateos, R. Molina, and A. K. Katsaggelos, "Variational Bayesian blind image deconvolution: A review," *Digital Signal Processing*, vol. 47, pp. 116–127, 2015.

[20] M. Hirsch, S. Sra, B. Scholkopf, and S. Harmeling, "Efficient filter flow for space-variant multiframe blind deconvolution," in *CVPR*, 2010, pp. 607–614.

[21] F. Šroubek and P. Milanfar, "Robust multichannel blind deconvolution via fast alternating minimization," *IEEE Trans. Image Process.*, vol. 21, pp. 1687–1700, 2012.

[22] H. Zhang, D. Wipf, and Y. Zhang, "Multi-observation blind deconvolution with an adaptive sparse prior," *IEEE Trans. Pattern Anal. Mach. Intell.*, vol. 36, pp. 1628–1643, 2014.

[23] M. J. Beal, *Variational algorithms for approximate Bayesian inference*, Ph.D. thesis, Univ. of London, 2003.

[24] J. Nocedal and S. J. Wright, *Numerical Optimization*, New York, NY: Springer New York, 1999.

[25] J.W Goodman, *Introduction to Fourier Optics*, Roberts and Company Publishers, 2005.

[26] L. Yujiri, M. Shourcri, and P. Moffa, "Passive millimeter-wave imaging," *IEEE Microwave Mag*, vol. 4, pp. 39–50, 2003.